AD-A032 067 HUGHES AIRCRAFT CO CULVER CITY CALIF AEROSPACE GROUP F/G 17/5
LOW COST ARRAYS FOR DETECTION OF INFRARED (LADIR).(U)
SEP 76 L M CANDELL, M Y PINES, W V BACKENSTO F33615-75-C-1175
UNCLASSIFIED HAC-P76-216 AFAL-TR-76-70 NL

1 OF 1
ADA032067

END

DATE
FILMED
1 -77

AFAL-TR-76-70

LOW COST ARRAYS FOR DETECTION IN INFRARED (LADIR)

AEROSPACE GROUPS
HUGHES AIRCRAFT COMPANY
CULVER CITY, CALIFORNIA 90230

SEPTEMBER 1976

INTERIM REPORT FOR PERIOD JANUARY 1975 - DECEMBER 1975

AIR FORCE AVIONICS LABORATORY
WRIGHT AERONAUTICAL LABORATORIES
AIR FORCE SYSTEMS COMMAND
WRIGHT-PATTERSON AIR FORCE BASE, OHIO 45433

NOTICE

When Government drawings, specifications, or other data are used for any purpose other than in connection with a definitely related Government procurement operation, the United States Government thereby incurs no responsibility nor any obligation whatsoever; and the fact that the government may have formulated, furnished, or in any way supplied the said drawings, specifications, or other data, is not to be regarded by implication or otherwise as in any manner licensing the holder or any other person or corporation, or conveying any rights or permission to manufacture, use, or sell any patented invention that may in any way be related thereto.

This report has been reviewed by the Information Office (OI) and is releasable to the National Technical Information Service (NTIS). At NTIS, it will be available to the general public, including foreign nations.

This technical report has been reviewed and is approved for publication.

William R. Woody

WILLIAM R. WOODY, Project Engineer
Electro-Optic Detectors Group
Electro-Optics Technology Branch

Donald J Peacock

DONALD J. PEACOCK, Actg. Chief
Electro-Optic Detectors Group
Electro-Optics Technology Branch

FOR THE COMMANDER

William C. Schoonover

WILLIAM C. SCHOONOVER, Chief
Electro-Optics Technology Branch
Electronic Technology Division

Copies of this report should not be returned unless return is required by security considerations, contractual obligations, or notice on a specific document.

AIR FORCE - 15 OCTOBER 76 - 100

UNCLASSIFIED

SECURITY CLASSIFICATION OF THIS PAGE *(When Data Entered)*

REPORT DOCUMENTATION PAGE	READ INSTRUCTIONS BEFORE COMPLETING FORM
1. REPORT NUMBER: AFAL-TR-76-70	2. GOVT ACCESSION NO.
3. RECIPIENT'S CATALOG NUMBER	
4. TITLE *(and Subtitle)*: LOW COST ARRAYS FOR DETECTION OF INFRARED (LADIR),	5. TYPE OF REPORT & PERIOD COVERED: Interim, January 1975 – December 1975
6. PERFORMING ORG. REPORT NUMBER: D3205 - P76-216	
7. AUTHOR(s): L. M. Candell, M. Y. Pines, W. V. Backensto	8. CONTRACT OR GRANT NUMBER(s): F33615-75-C-1175
9. PERFORMING ORGANIZATION NAME AND ADDRESS: Aerospace Groups, Hughes Aircraft Company, Culver City, California 90230	10. PROGRAM ELEMENT, PROJECT, TASK AREA & WORK UNIT NUMBERS: 35 p.
11. CONTROLLING OFFICE NAME AND ADDRESS: Air Force Avionics Laboratory (DHO-3), Air Force Wright Aeronautical Laboratories (AFSC), Wright-Patterson AF Base, Ohio 45433	12. REPORT DATE: Sep[illegible]76
	13. NUMBER OF PAGES: 29
14. MONITORING AGENCY NAME & ADDRESS *(if different from Controlling Office)*: HAC-P76-216, HAC-D3205	15. SECURITY CLASS. *(of this report)*: Unclassified
	15a. DECLASSIFICATION/DOWNGRADING SCHEDULE

16. DISTRIBUTION STATEMENT *(of this Report)*

Approved for public release; distribution unlimited.

17. DISTRIBUTION STATEMENT *(of the abstract entered in Block 20, if different from Report)*

Interim rept. Jan-Dec 75,

18. SUPPLEMENTARY NOTES

19. KEY WORDS *(Continue on reverse side if necessary and identify by block number)*

Extrinsic silicon detectors
Charge coupled devices (CCD)
Detector crosstalk
Monolithic focal planes
Time delay and integration (TDI)
Electronic readout (ERO)

20. ABSTRACT *(Continue on reverse side if necessary and identify by block number)*

Data is presented in discrete Si:Ga detectors, monolithic detectors and test structures on the 2096 chip, and preliminary design of the 21xx test chip.

DD FORM 1 JAN 73 1473 EDITION OF 1 NOV 65 IS OBSOLETE

UNCLASSIFIED

SECURITY CLASSIFICATION OF THIS PAGE *(When Data Entered)*

172 310

PREFACE

This interim report describes the results of the Low Cost Array for Detection of Infrared (LADIR) program from May 1975 through December 1975. The objective of LADIR is to investigate monolithic Si:Ga detector arrays for 8 to 14 μm infrared imaging with on-chip signal processing. This report describes the key results of tests performed on discrete Si:Ga detectors, monolithic Si:Ga detectors and detector/CCD test structures on the Hughes 2096 IR &D test chip.

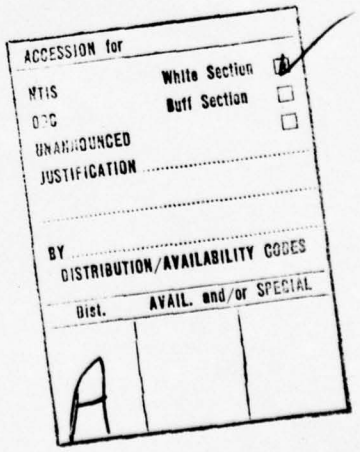

CONTENTS

LIST OF ILLUSTRATIONS

SECTION I
INTRODUCTION

The LADIR contract is a device development/evaluation program to investigate monolithic extrinsic (Si:Ga) detector arrays for 8 to 14 μm IR imaging systems with on chip signal processing functions. The objective is to demonstrate solutions to critical device performance questions prior to the development of a fully monolithic focal plane assembly which will be undertaken during a follow-on phase. The contract requires the evaluation and delivery of monolithic focal plane arrays, preamplifier arrays, multiplexer arrays, direct/indirect CCD injection schemes and a preliminary MFPA. These contract objectives are to be achieved by testing specific applicable devices on the 2096 chip, design and development of a dedicated test chip (21XX), and by testing discrete Si:Ga detectors to select optimum dopant concentration for 21XX substrate material.

This report describes the key results of tests performed on discrete Si:Ga detectors, monolithic detectors and test structures on the 2096 chip and the preliminary design of the 21XX test chip.

SECTION II
DISCRETE DETECTORS

Several discrete float zone grown detector elements having different dopant levels were fabricated. Frequency response measurements were made on the 3009 A Tang material under three different background conditions utilizing a PbSnTe laser. The results are shown in Figure 1,* which demonstrates that the high frequency response characteristics of Si:Ga detectors are as theoretically predicted. That is to say, the frequency response decreases as the background decreases. D^* as a function of temperature is presented in Figure 2 for three different phosphorous doping levels at three different backgrounds. This data shows that the detectors will operate optimally up to 32°K theoretically but only 27°K experimentally. The experimental and theoretical data correlates reasonably well. Figure 3 shows D^*

*All figures appear at the end of the text, beginning on page 6, preceding the Appendix.

data as a function of temperature at a high background level for three different gallium concentrations, keeping P essentially constant. The roll-off in D^* at the low temperature is believed to be due to the contact limitations. Different contacts are used on monolithic structures. This data indicates that higher D^* may be obtained with larger concentrations of gallium. A complete discussion of the characteristics of the gallium doped silicon detectors is given in the Appendix.

SECTION III
MONOLITHIC DETECTORS

A picture of the 2096 chip is shown in Figure 4 showing the various test circuits tested. This chip contained five individual monolithic detectors that are adjacent but spaced at different center-to-center spacings to allow the effects of the spacing variable to be evaluated. Figure 5 shows crosstalk measurements made on these devices. The results are very encouraging. Measured crosstalk was less than 5 percent for all devices except the center detector which was noisy.

The spectral response of one of the monolithic detectors was obtained and shown in Figure 6. The dip at 3 μm is not presently understood. The peak wavelength is 14 μm and the cut-off wavelength is 17.2 μm.

A significant amount of data was obtained on the discrete 2096 detectors. Figure 7 shows signal response at 1.1×10^{17} ph/cm^2/sec. The 3 dB frequency is approximately 900 kHz and decreases as the bias voltage increases. The signal level increases, as expected, with bias. Figure 8 shows the output noise spectra. From the ratio of signal to noise in Figures 7 and 8, f^* is in excess of 1 MHz. D^* is calculated to be 5.6×10^{10} cm$\sqrt{\text{Hz}}$/w which translates to a quantum efficiency of 0.29. The theoretical expectation is 0.33.

Data was also obtained at a background of 1.5×10^{14} ph/cm^2/sec. Figure 9 shows the signal and output noise spectra. The signal 3 dB frequency is approximately 170 kHz. f^* is in excess of 250 kHz. D^* at this background is shown in Figure 10. Peak D^* is 1.4×10^{12} cm$\sqrt{\text{Hz}}$/w which means a quantum efficiency of 0.23, somewhat lower than the 1.1×10^{17} background quantum efficiency. Figure 11 shows the impulse response obtained from a PbSnTe laser at the 1.5×10^{14} background.

SECTION IV
INPUT TEST STRUCTURES

Also available on the 2096 chip were various input schemes designed to demonstrate which type is best. Figures 12 and 13 show the normal direct injection structure and an equivalent circuit. This input structure is characterized by a current dependent input transconductance which limits the available system bandwidth. To eliminate this problem several modified direct injection circuits have been designed. Several of these structures were evaluated to determine if the new structures would provide better frequency response in the absence of the input g_m problem of the normal direct injection, and to determine the optimum type of detector contact.

Figure 14 shows D^* obtained with these input structures at a background of 2×10^{16} ph/cm^2/sec. The signal data was obtained with a PbSnTe laser emitting at 10.8 μm. Input No. 4 is a new structure with a p^+ buried layer contact. Input No. 6 is a new biased structure but does not have a p^+ contact. Input No. 1 is the normal p^+ direct injection structure. Input No. 4 appears to be the best from this preliminary data. BLIP operation was achieved, assuming 0.36 quantum efficiency with an f^* greater than 200 kHz. Figure 15 shows the impuse response to a PbSnTe laser pulse. From this response the 3 dB signal response appears to be about 40 kHz.

Data was also taken on the input test structures at a background of 1.5×10^{14} ph/cm/sec. Figure 16 shows D^* for the same input structures, Nos. 1, 4 and 6. One can see that f^* is significantly improved with the new structures at the lower background. BLIP operation is achieved, assuming a quantum efficiency of 0.175 and f^* appears to be near 100 kHz.

SECTION V
TDI AND MULTIPLEXER RESULTS

The 2096 chip contained a 16-input TDI circuit which was utilized to demonstrate operation of TDI at LADIR backgrounds, and it was also used to demonstrate operation of a multiplexer. Figure 17 shows a schematic of the 16 input structure which had a standard p^+ direct injection input and a floating diffusion source follower output. Figure 18 shows the distinction between operating this structure in TDI or as a multiplexer. In TDI the blur circle is scanned along the detectors at the same speed as the clock so that charges

are added up. In the multiplexer mode the detectors are irradiated simultaneously and then read out serially. This is also known as an electronic readout (ERO) output. Figure 19 shows an example of the multiplexer readout at 1.3×10^{17} ph/cm^2/sec. Figure 20 shows an example at 1.6×10^{16} ph/cm^2/sec. These pictures confirm that high uniformity is achievable with current processing and materials technology. This chip was shielded to define the active detector area and resulted in improved uniformity over previously unshielded samples. Figure 21 shows an example of TDI readout. D^* was calculated for the 16 input TDI structure at backgrounds of 1.3×10^{17} ph/cm^2/sec and 1.6×10^{16} ph/cm^{2}sec. These calculations are shown in Figures 22 and 23. At 1.3×10^{17} ph/cm^2/sec, BLIP operation was achieved at 25°K with a quantum efficiency of 0.30. f^* was approximately 25 kHz. At 1.6×10^{16} ph/cm^2/sec, BLIP operation was achieved at 20°K, also with a quantum efficiency of approximately 0.30 and an f^* of about 25 kHz.

SECTION VI
DEEP BURIED CHANNEL CCD

The 2096 chip also contains a deep buried channel CCD. It is an n-buried layer device (n epi) designed to operate at the very high clock frequencies (up to 100 MHz) required on the future LADIR system. The n channel is best for high frequency operation because the mobility of electrons is much greater than that of holes. Preliminary results are that the deep buried channel does operate at 20°K at 15 MHz. Figure 24 shows pictures of operation at various temperatures at 15-MHz clock frequency. The top trace is the input pulse and the bottom trace shows the clock pulses and the output signal which is inverted due to the inverting output. Coupling existed between the input and output, however, which prevented meaningful signal-to-noise data from being taken. New devices have been fabricated with the input and output isolated and will soon be tested.

SECTION VII
NEW LADIR CHIP DESIGN

The new LADIR chip is currently being designed and layed out by the Hughes Carlsbad Research Center. A schematic of the proposed LADIR

chip is shown in Figure 25. One of the major items is the 49-row MFPA structure. There will be 10 detectors in TDI in each row for a total of 490 detectors. There will also be several test structures on the new chip such as a detector/buffer/gate modulation TDI structure, which will demonstrate the increased signal bandwidths obtainable with a MOSFET buffer preamp.

In addition a modified direct injection TDI structure will be provided which will demonstrate whether improved signal response is attainable with this structure as indicated by tests on the 2096 chip.

High frequency deep buried channel multiplexers will be provided, designed to operate at 30 MHz, which will be compared with a surface channel multiplexer to demonstrate whether there is significant improvement with deep buried layer performance. There will be a combination surface channel shift register and a deep buried channel multiplexer to demonstrate whether this combination is possible, since it will be ultimately necessary. Various MUX output schemes will be provided such as running three multiplexers in parallel so as to cut down the required MUX clock frequency.

In addition, there will be high resistance load resistors to provide information on uniformity. Large geometry FETS will be included for charge pumping measurements to measure the surface state density and surface mobilities. Discrete detectors will also be provided to characterize the detectors and check the processing.

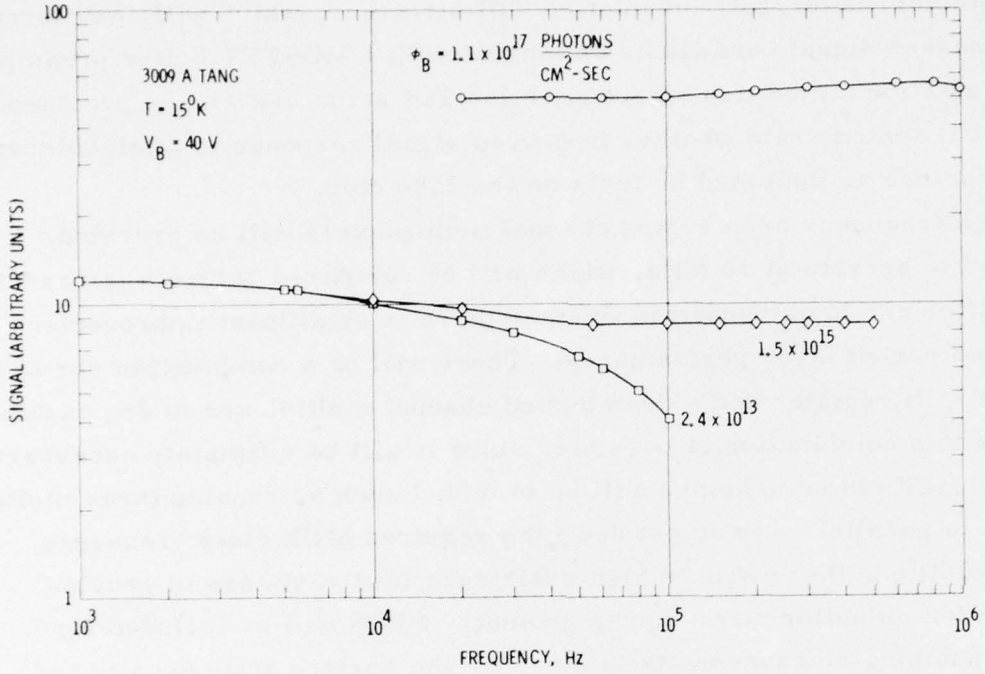

Figure 1. Si:Ga signal response versus frequency — PbSnTe laser source

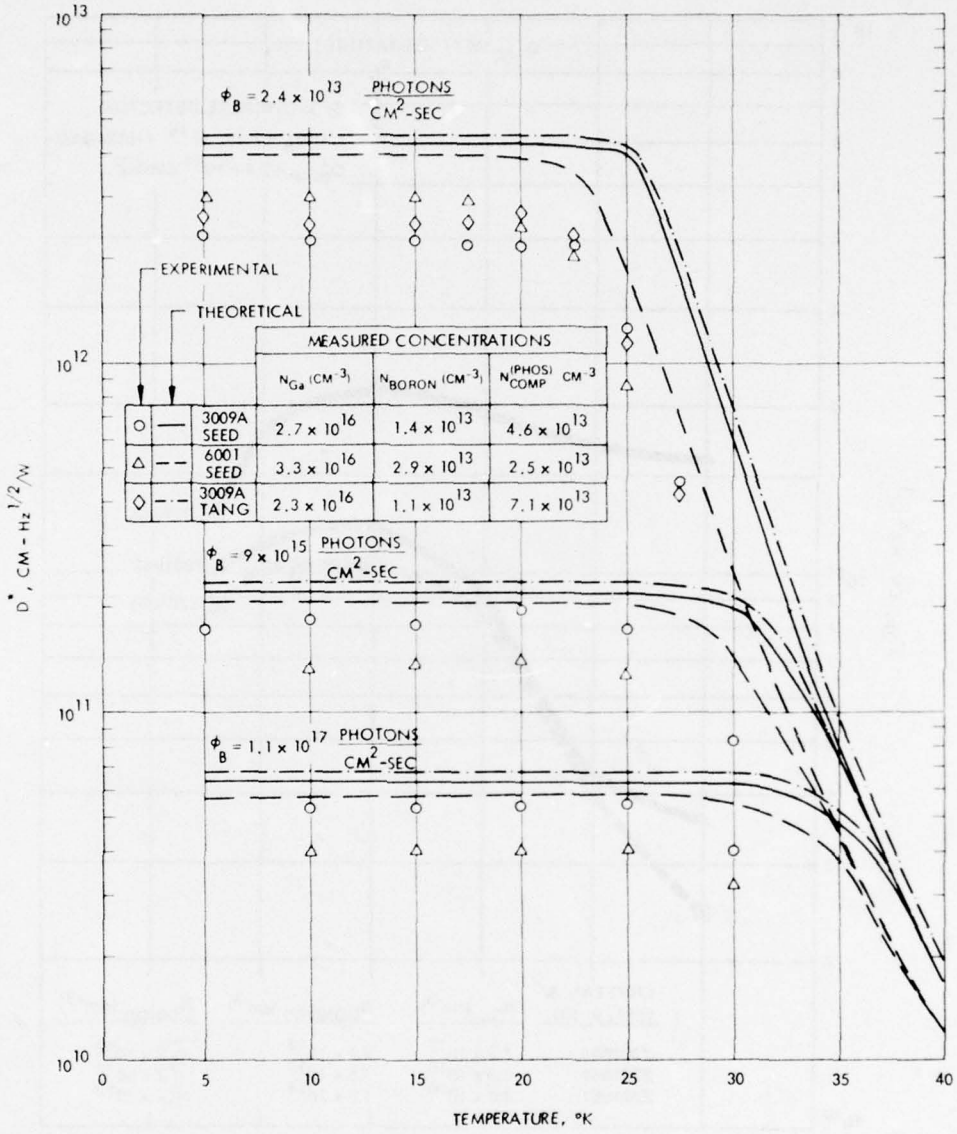

Figure 2. D^* as a function of temperature for various background photon flux densities

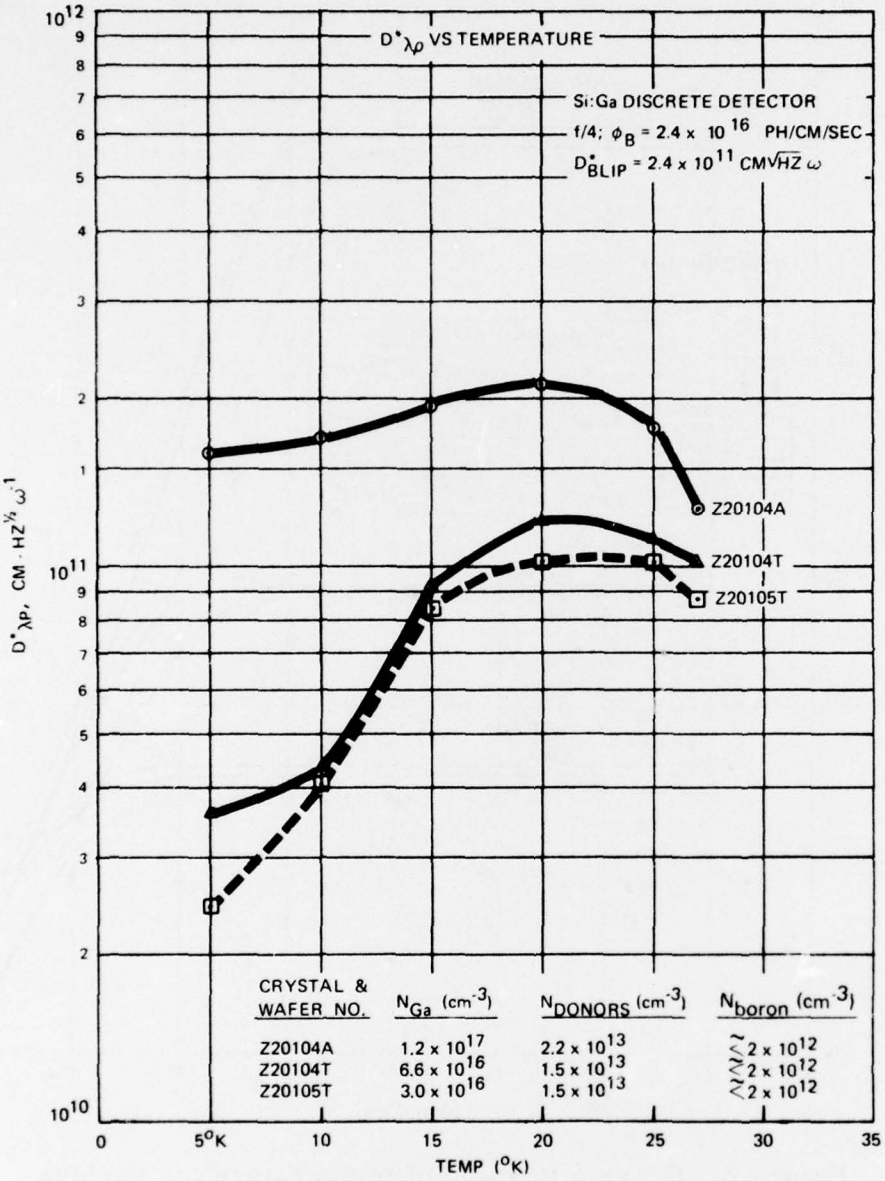

Figure 3. D* as a function of temperature for various gallium doping levels

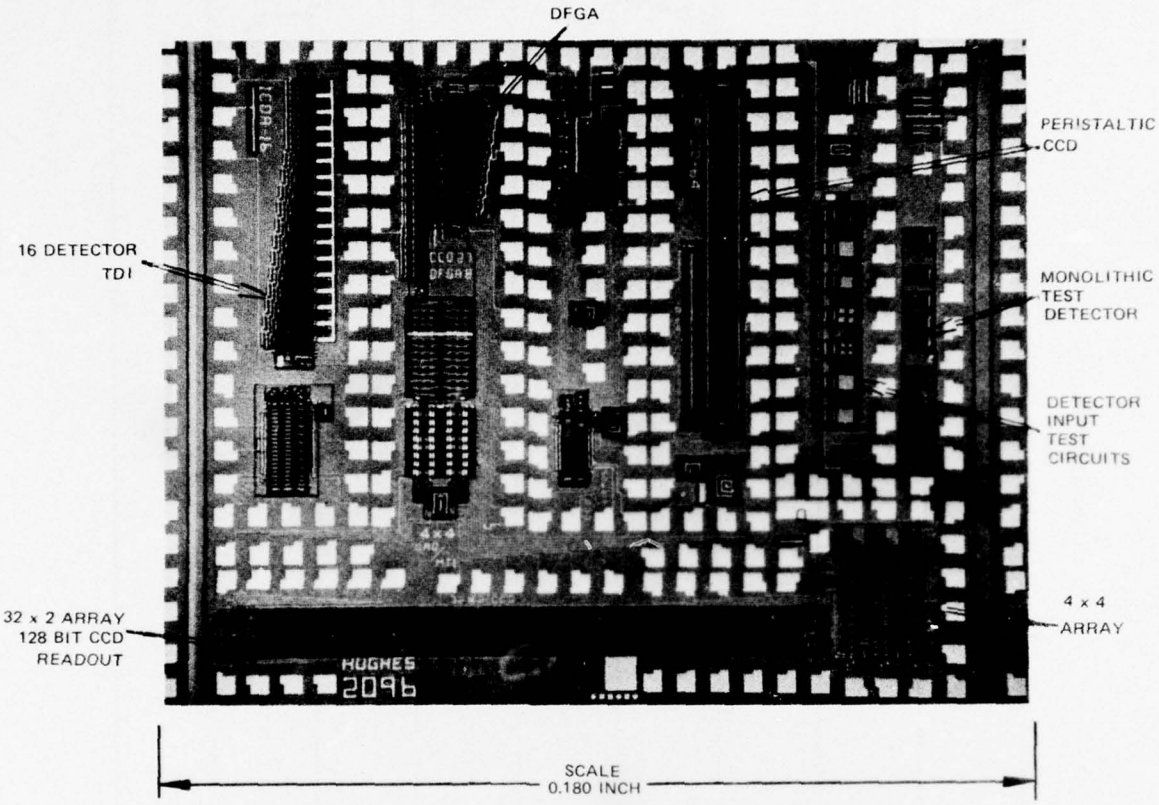

Figure 4. Extrinsic silicon test chip 2096

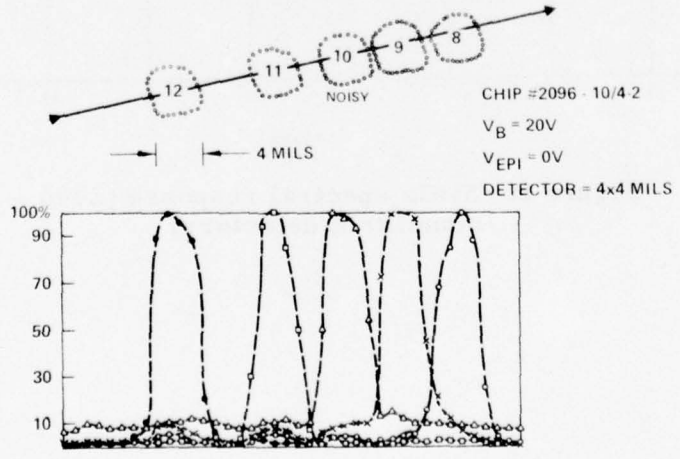

Figure 5. Extrinsic silicon 2096 chip — crosstalk measurements

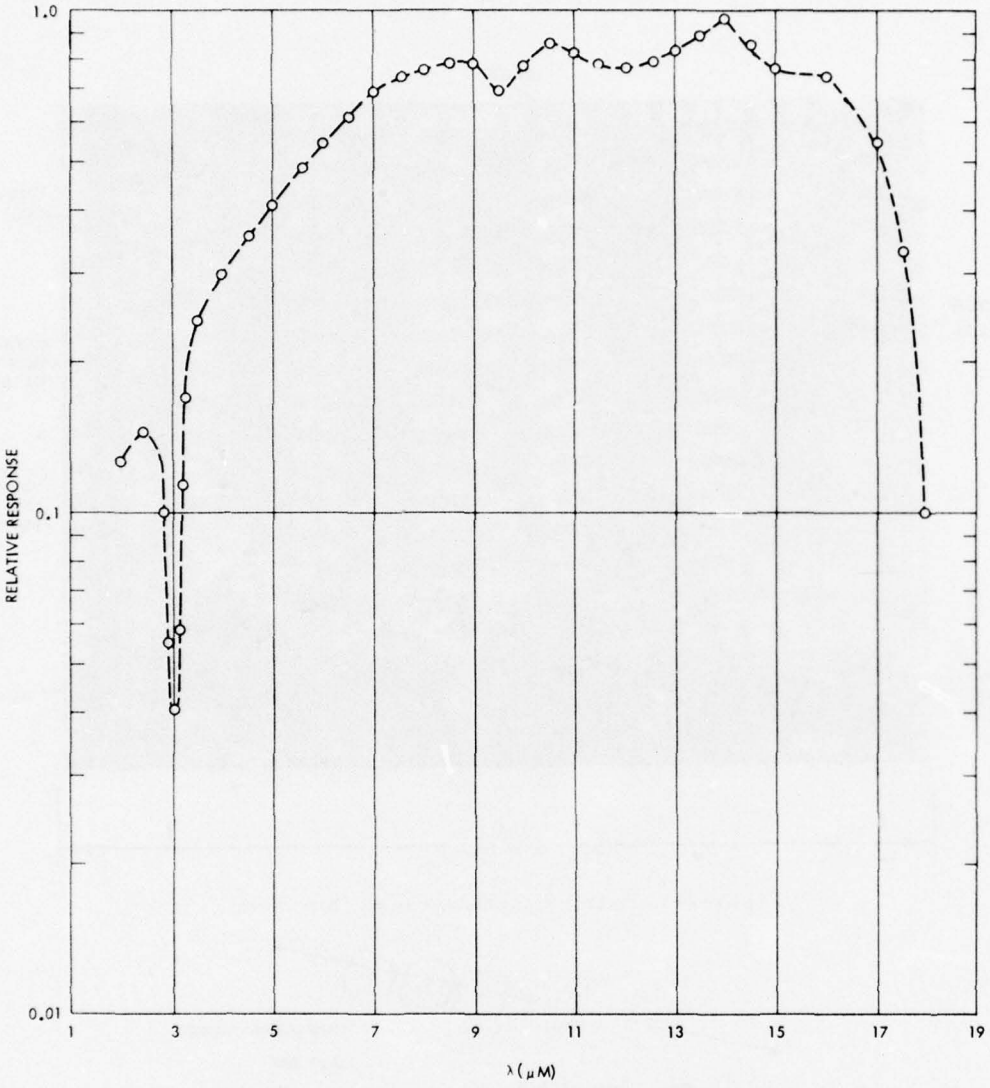

Figure 6. Si:Ga spectral response (2096 – 10/4 monolithic detectors)

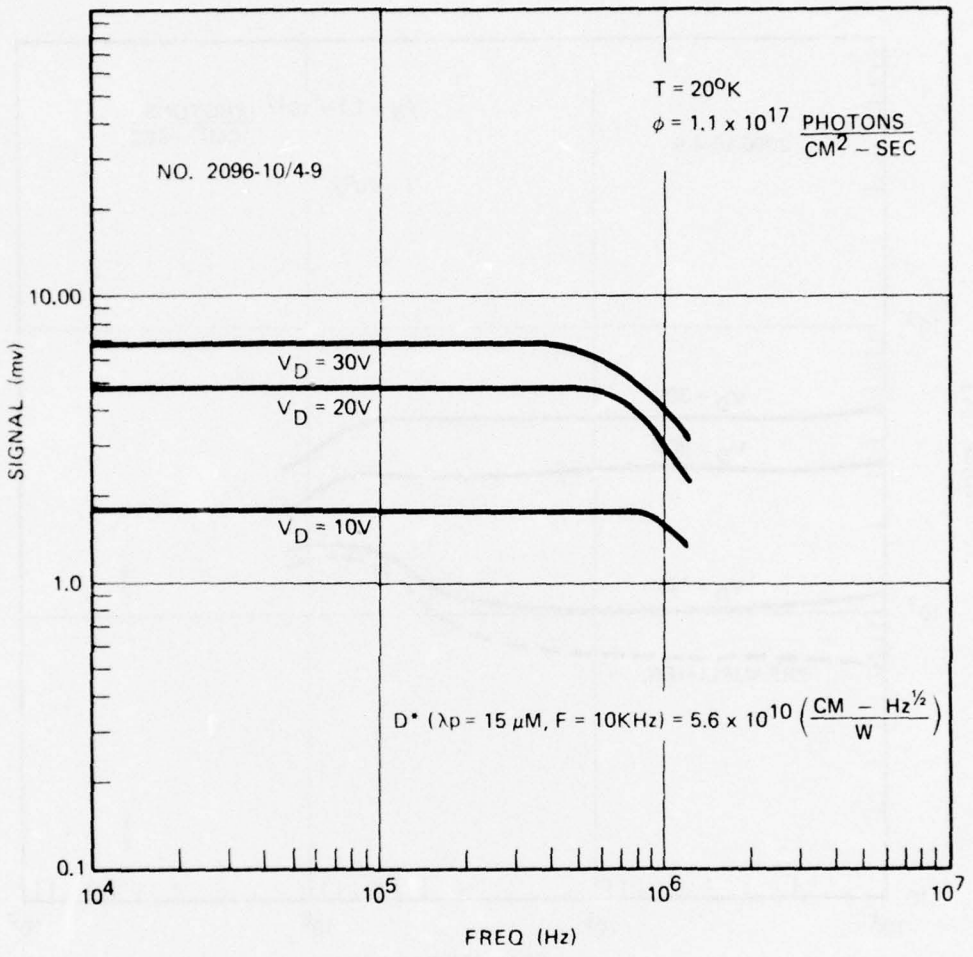

Figure 7. Si:Ga monolithic detector signal versus frequency

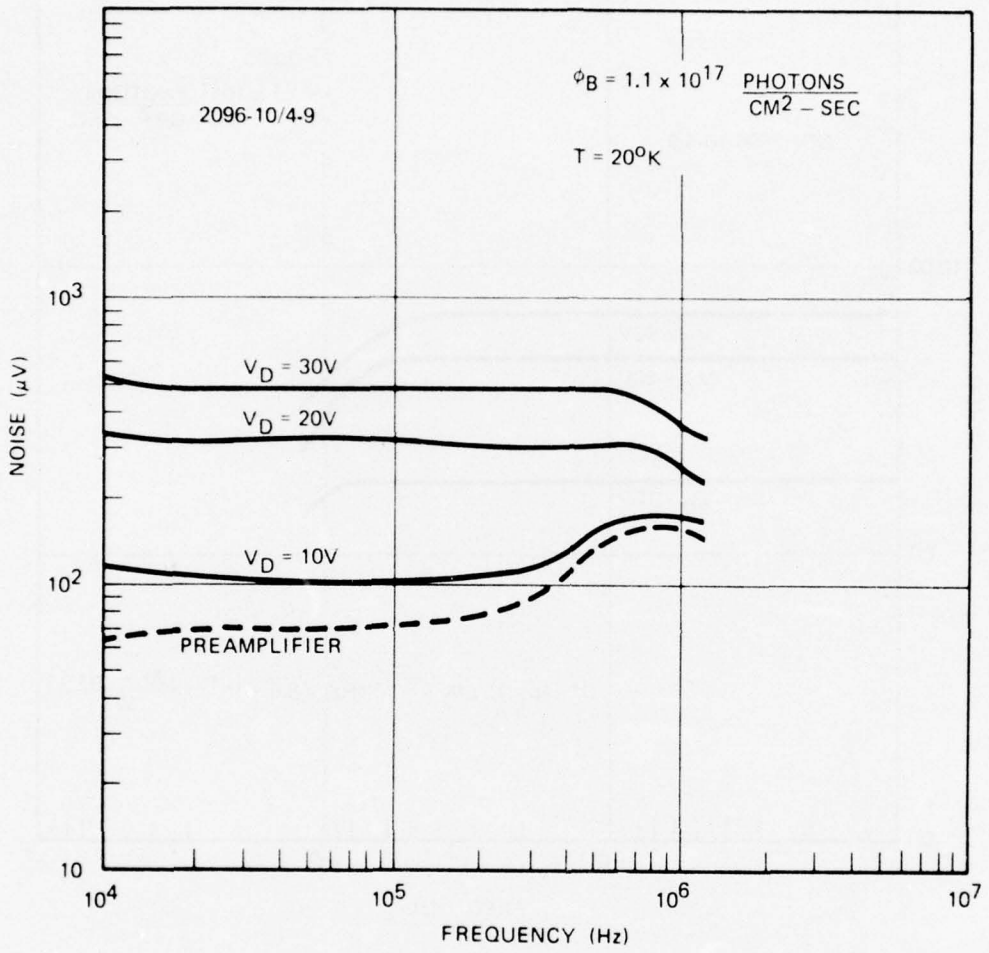

Figure 8. Si:Ga monolithic detector – output noise versus frequency

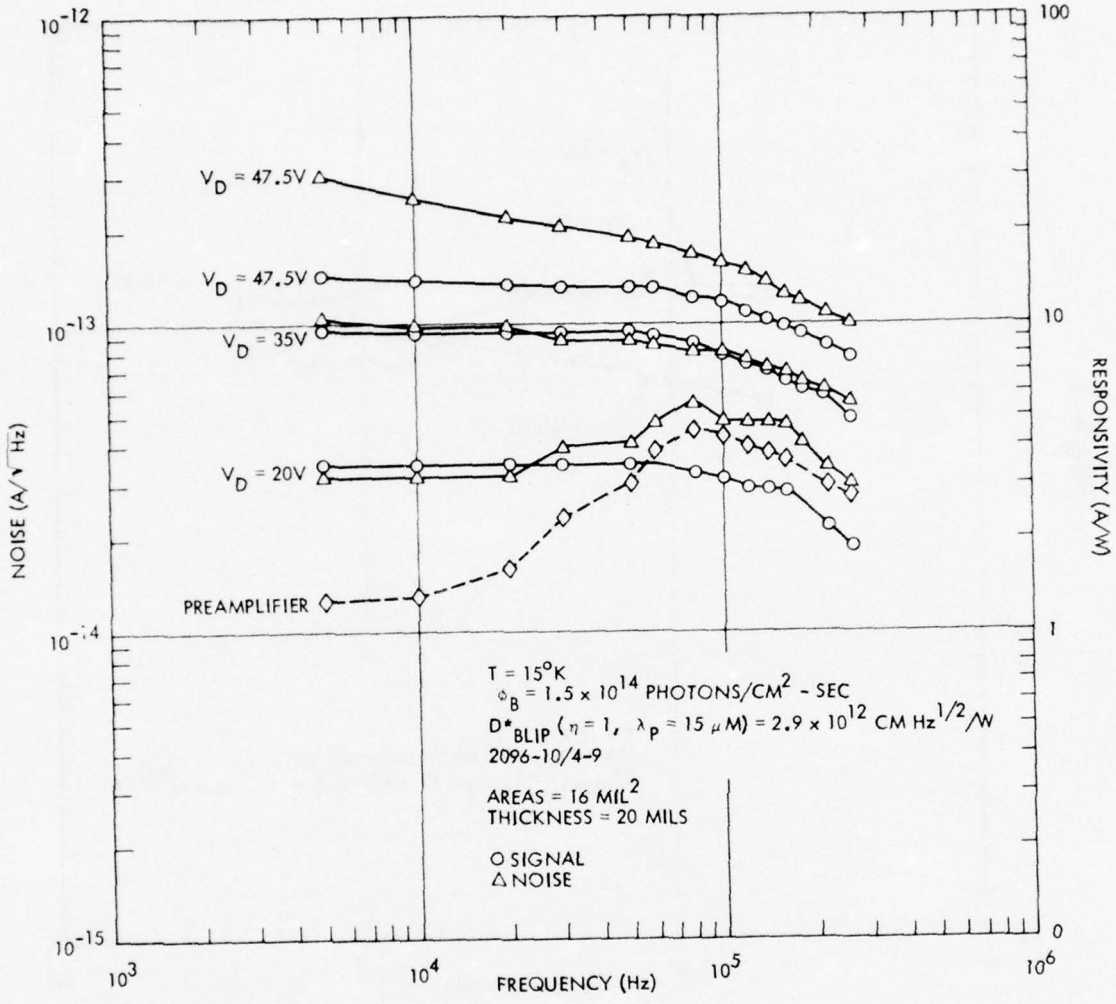

Figure 9. Si:Ga 2096 extrinsic silicon chip monolithic detector, responsivity and noise versus frequency

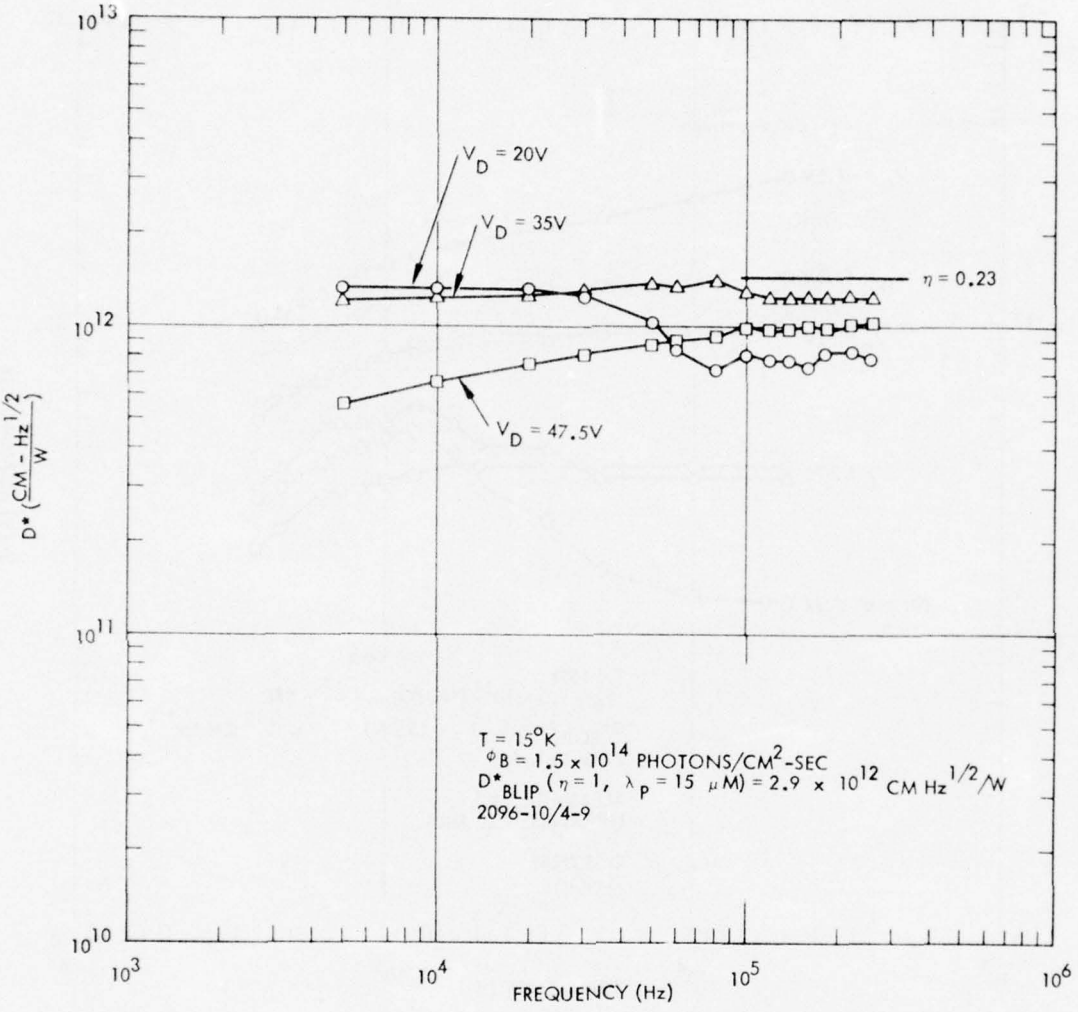

Figure 10. Si:Ga 2096 chip monolithic detector, D^* versus frequency

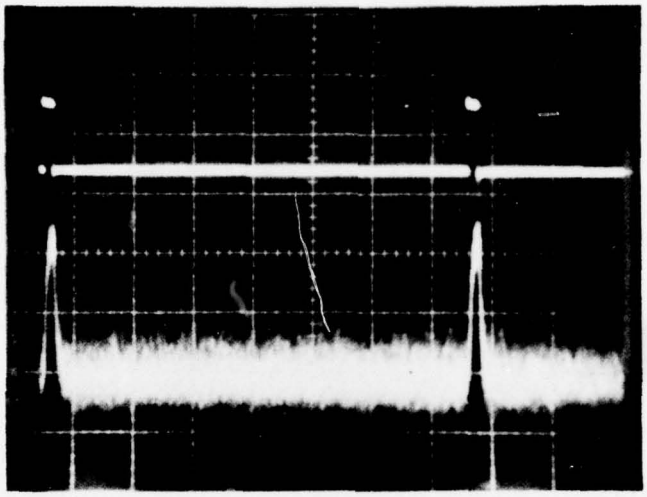

TIME = 5 μS/DIVISION
0.1 V/DIVISION – SIGNAL
1 V DIVISION – LASER

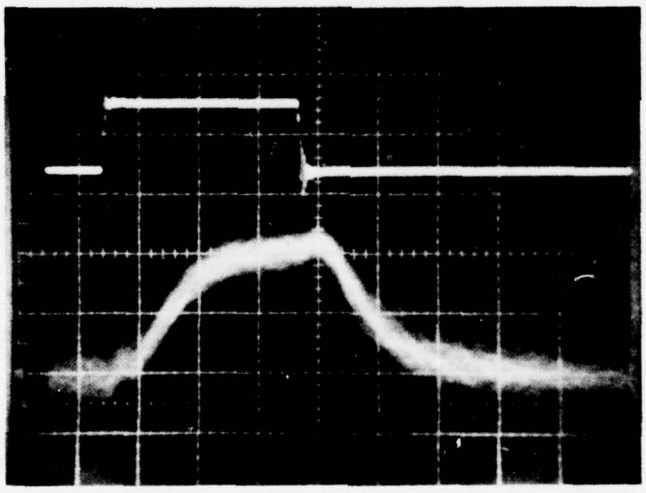

TIME = 1 μS/DIVISION
0.1 V/DIVISION – SIGNAL
1 V/DIVISION – LASER

Figure 11. PbSnTe laser pulse, Si:Ga discrete monolithic detector on 2096, 10/4-8 ($\phi_B = 1.5 \times 10^{14}$ ph/cm^2-sec)

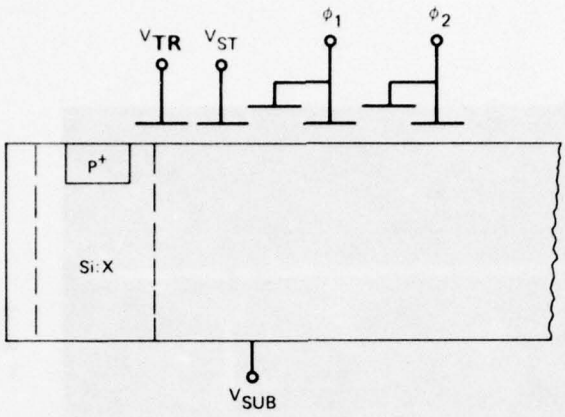

Figure 12. Si:x normal direct injection structure

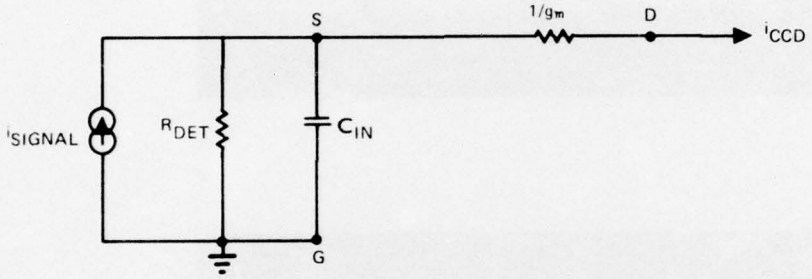

Figure 13. Si:x normal direct injection equivalent circuit

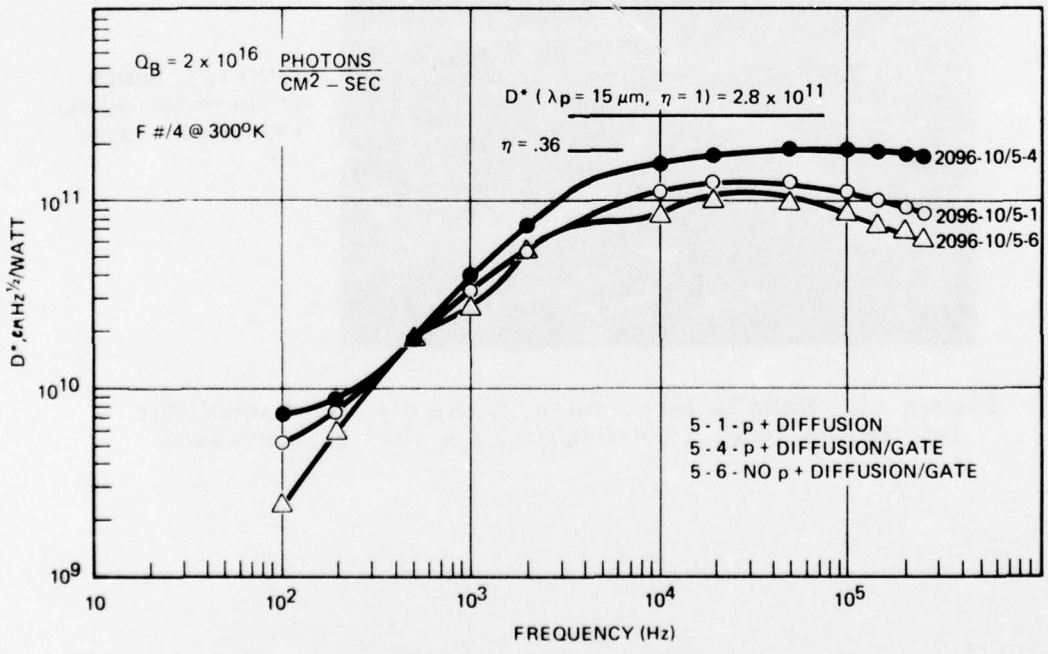

Figure 14. Si:Ga 2096 chip-CCD input structure, D^* versus frequency

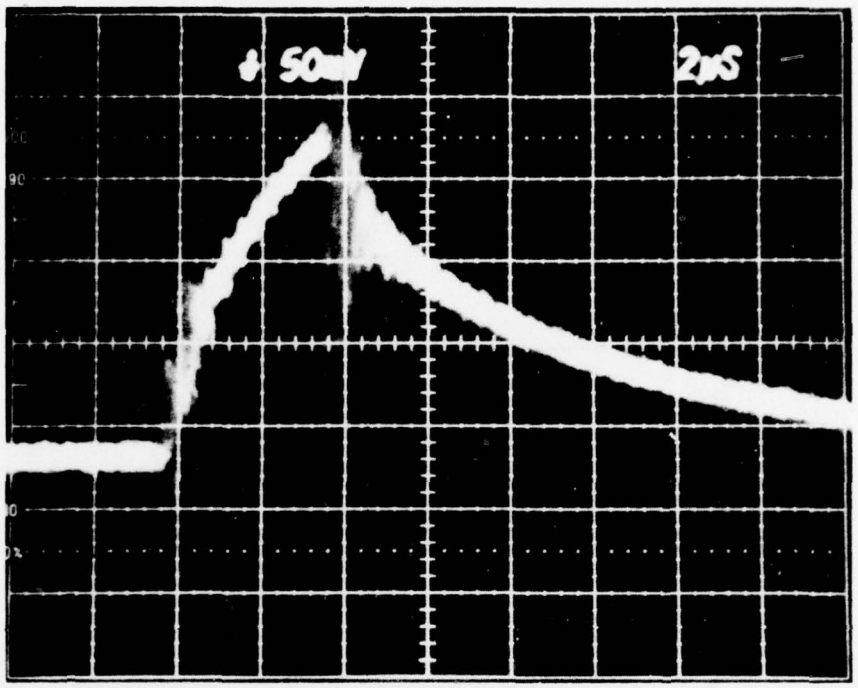

2 μS/DIVISION

PbSnTe LASER 10.8 μM
DETECTOR NO.4

$Q_B = 2 \times 10^{16}$ PH/CM^2/SEC
T = 10°K

Figure 15. CCD 2096 - 10/4-4, laser pulse response

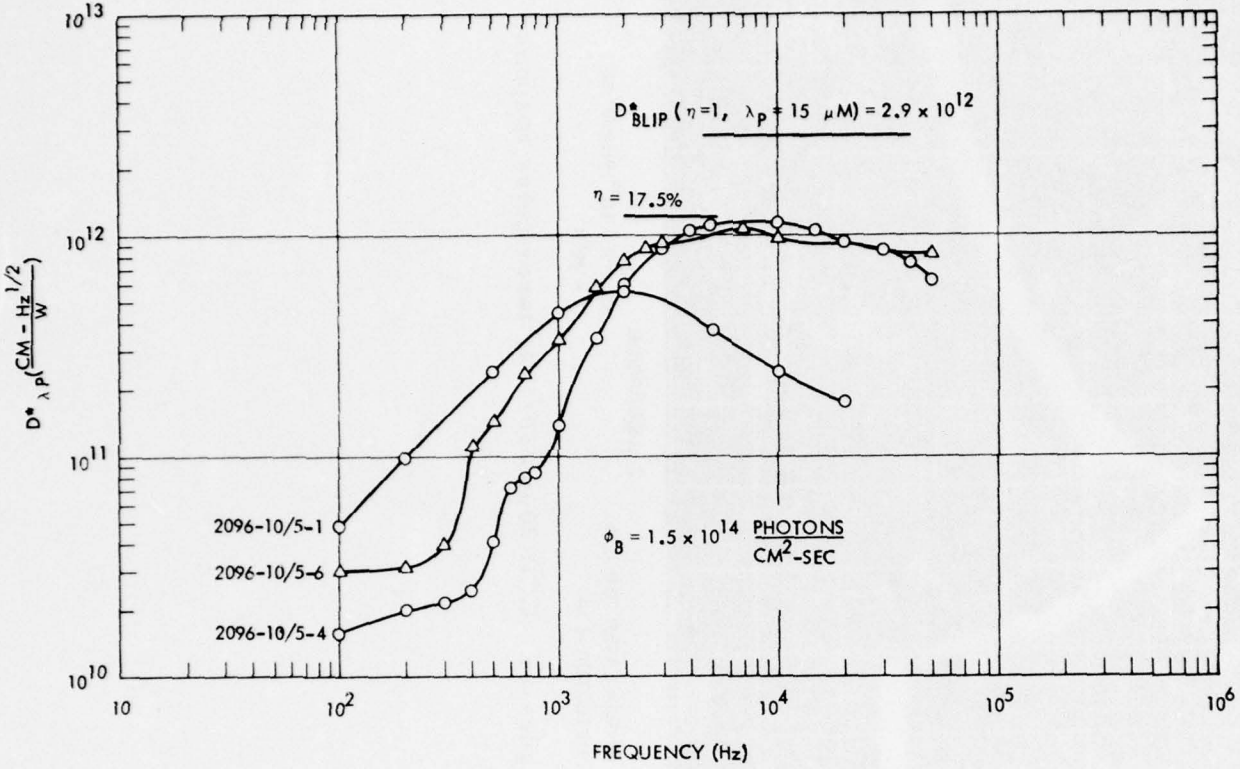

Figure 16. CCD input structure, 2096 extrinsic silicon chip D^* versus frequency

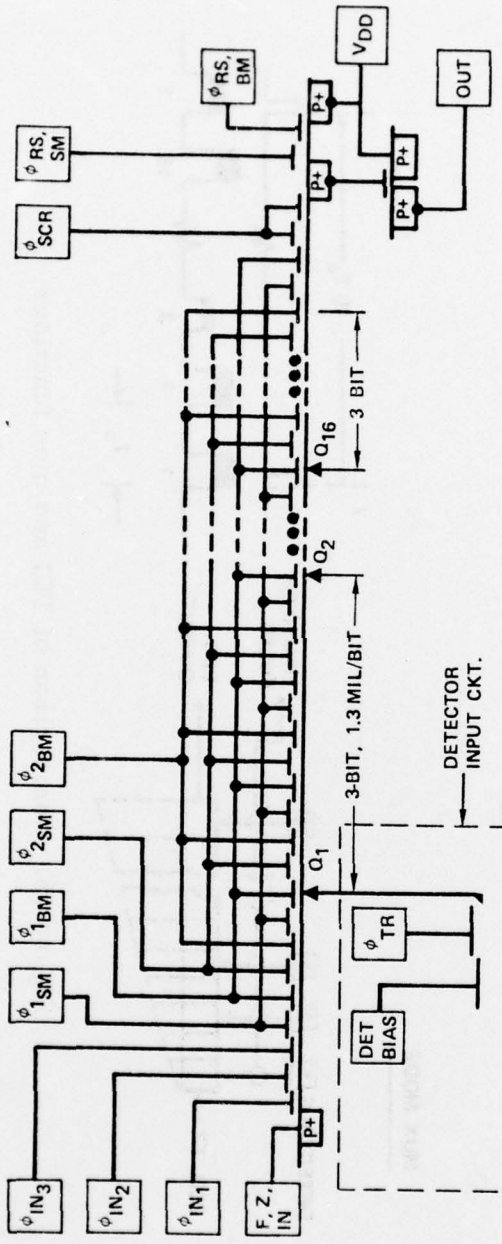

Figure 17. Six test chip 2096

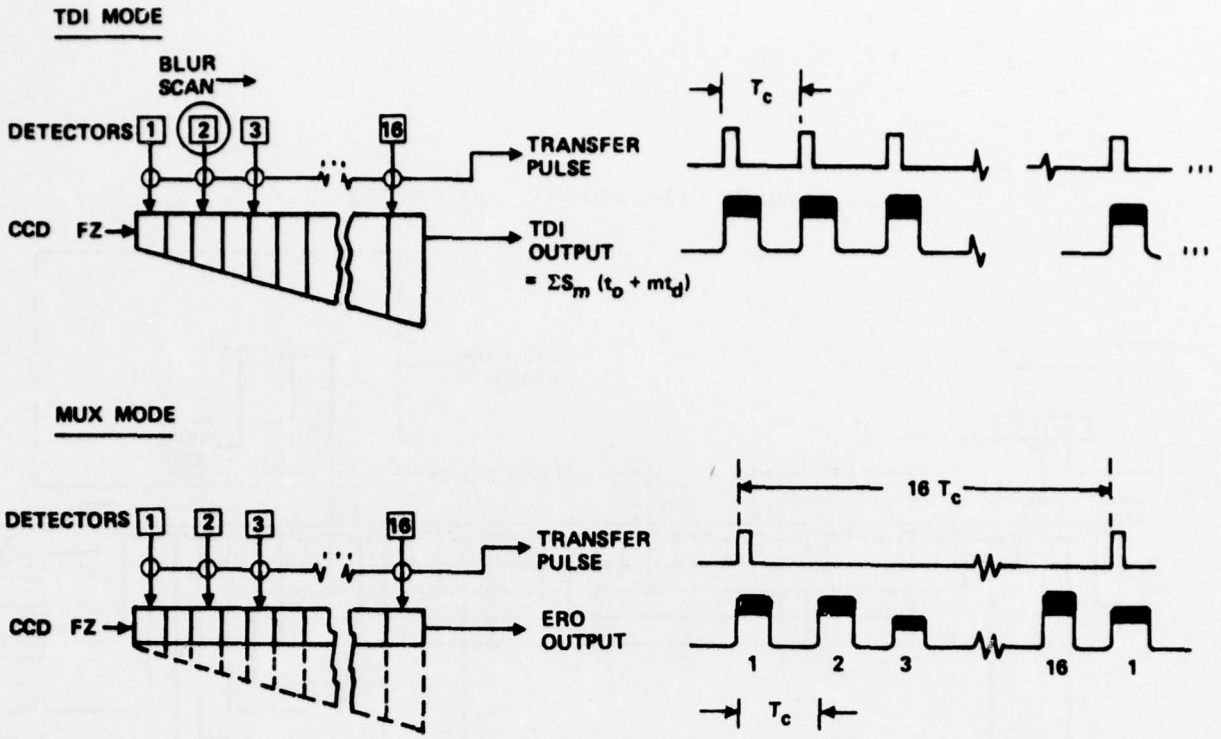

Figure 18. Comparison of TDI and mux functions

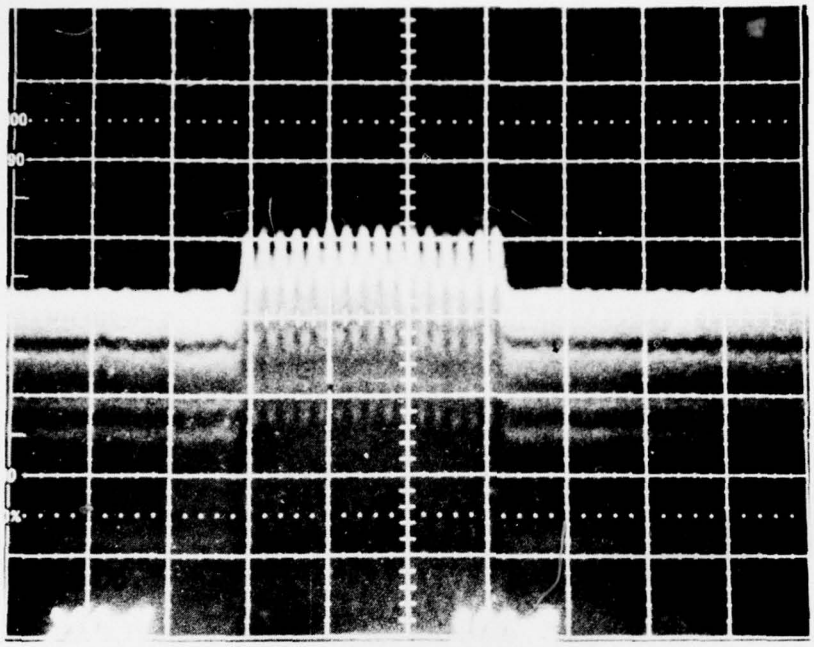

LOT 10, WAFER 3
CHIP No. D–1
CLOCK = 200 kHz
TEMP = 20°K
ϕ_B = 1.3 x 10^{17} PH/CM^2-SEC

Figure 19. 2096 chip mux readout

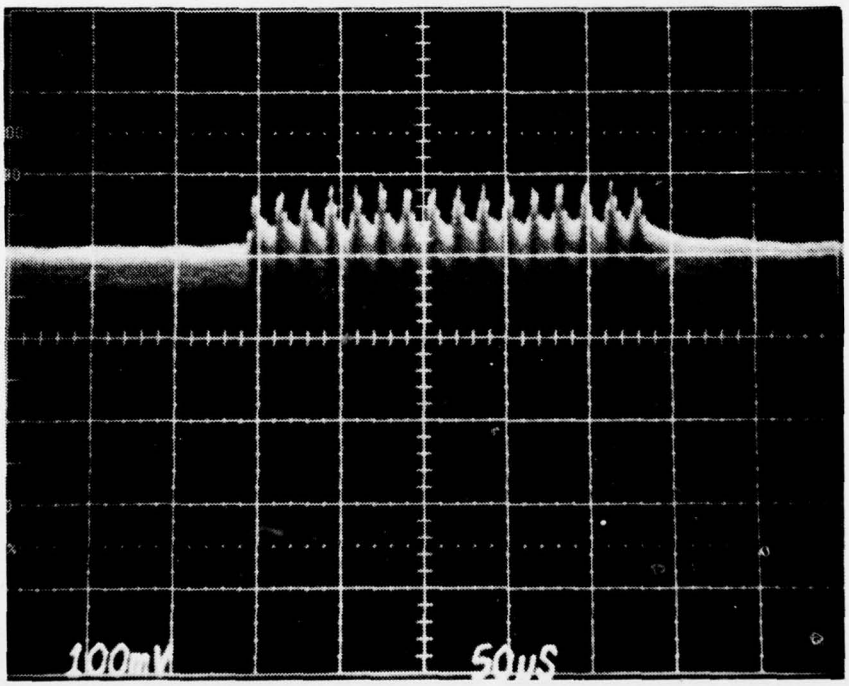

LOT 10, WAFER 3
CHIP NO. F
CLOCK = 200 kHz
TEMP = 20°K
ϕ_B = 1.6 x 10^{16} PH/CM^2/SEC

Figure 20. 2096 chip mux readout

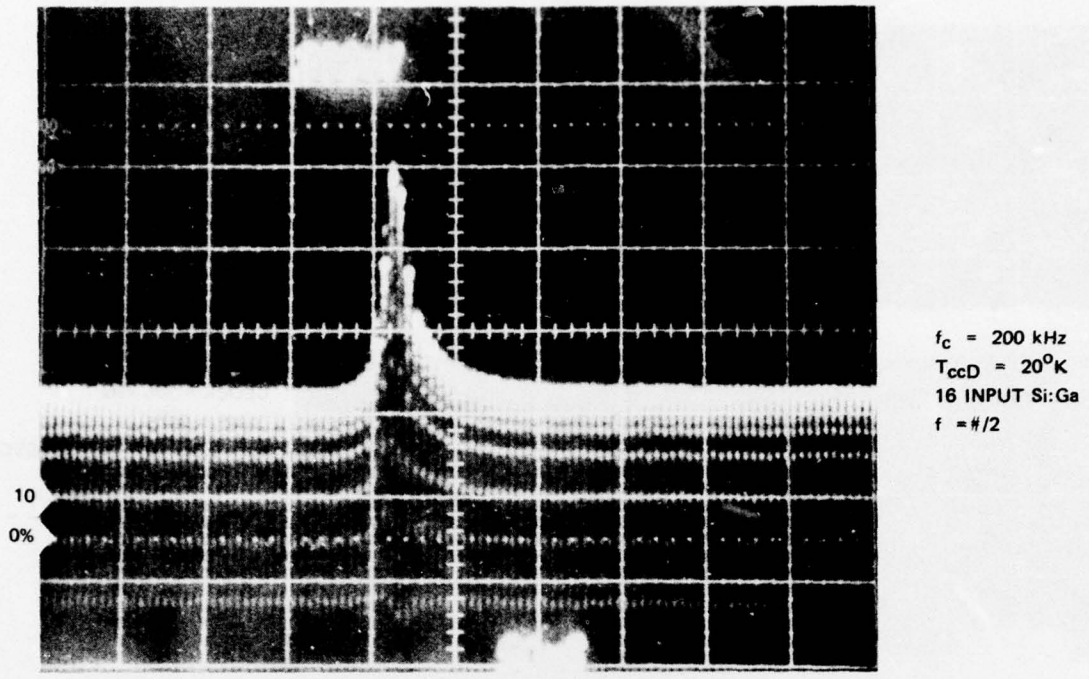

Figure 21. Extrinsic silicon 2096 chip-TDI output

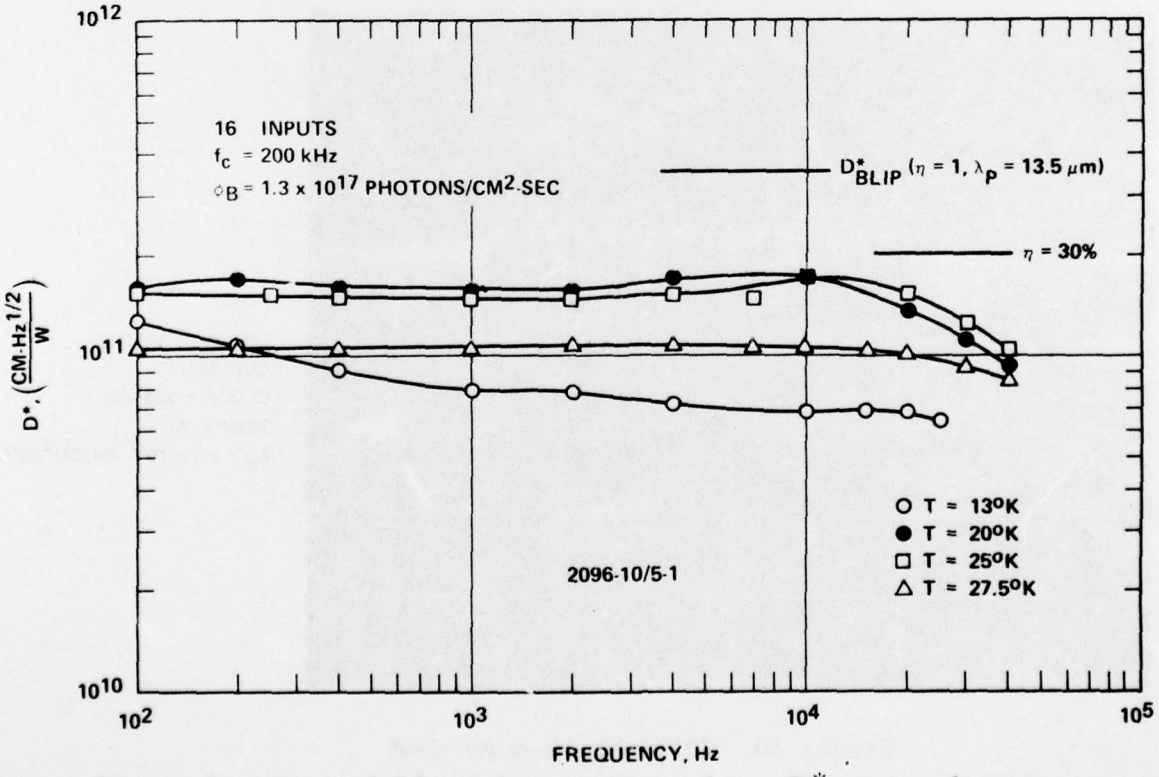

Figure 22. Si:Ga 2096 extrinsic silicon chip - D^* versus frequency

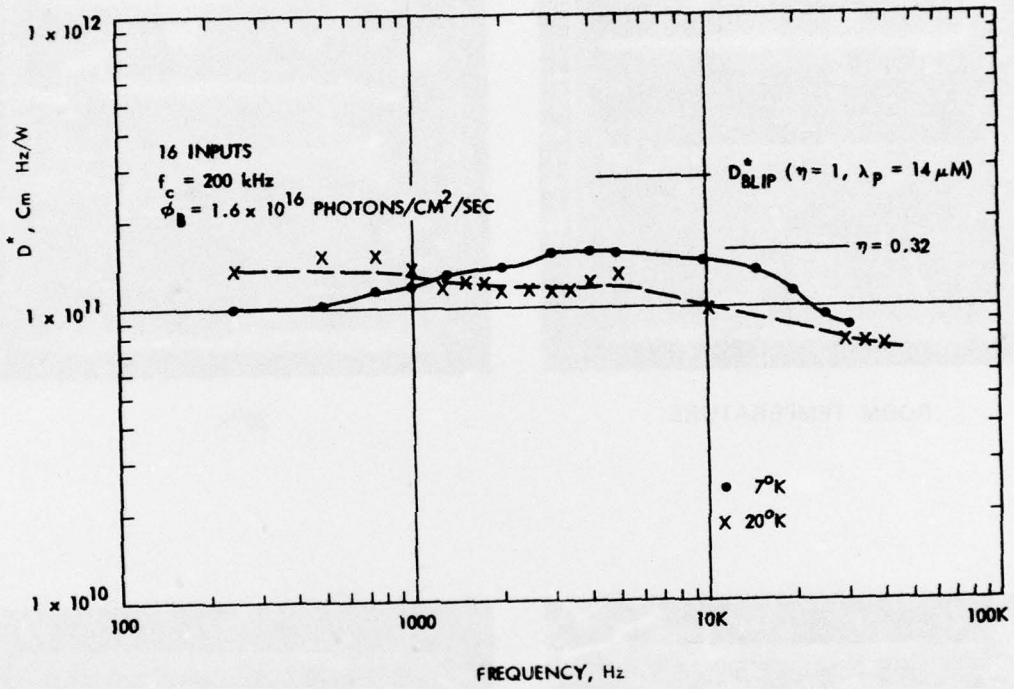

Figure 23. Si:Ga 2096 chip, D^* versus frequency

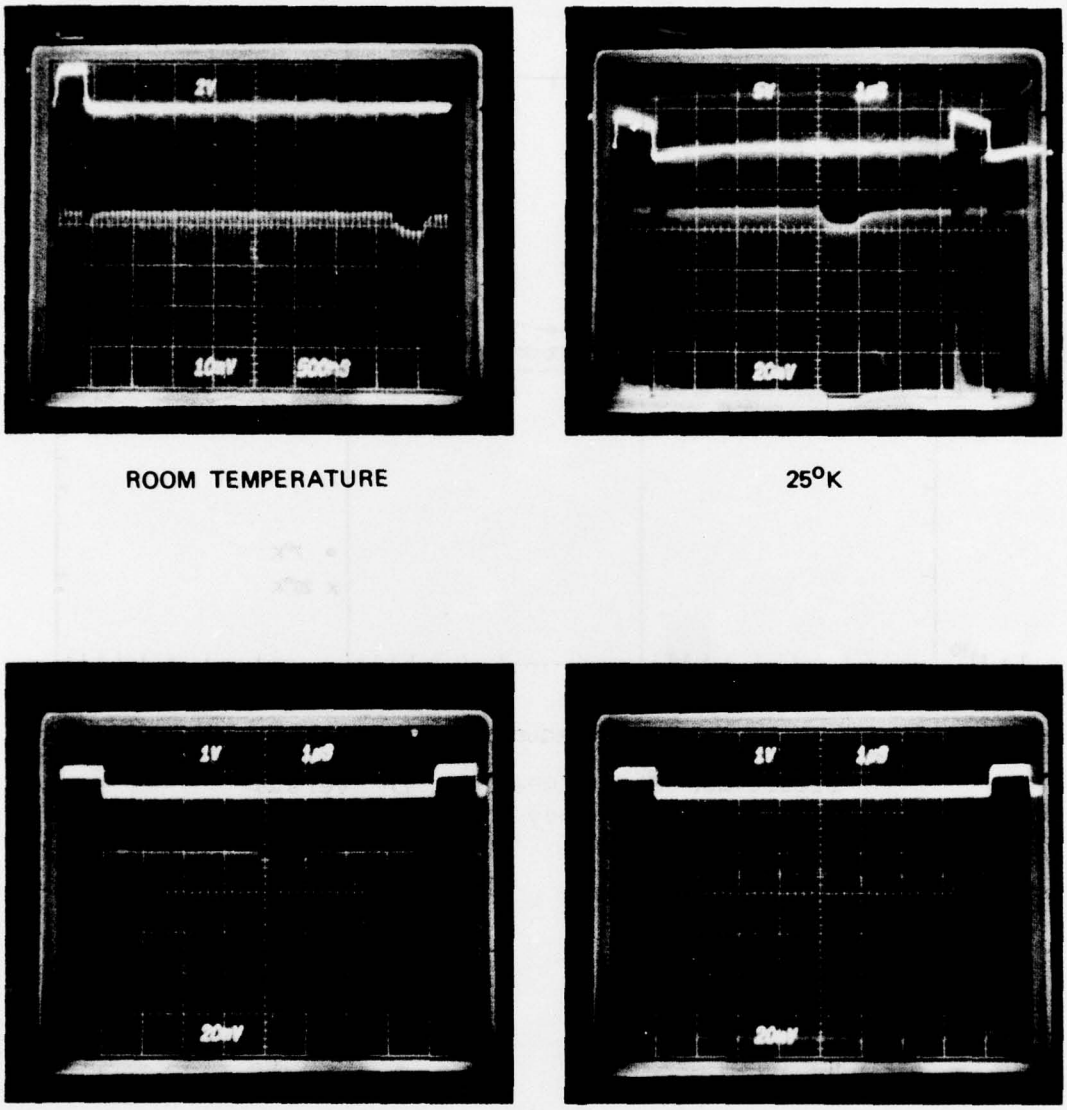

Figure 24. 2096 deep buried layer CCD mux

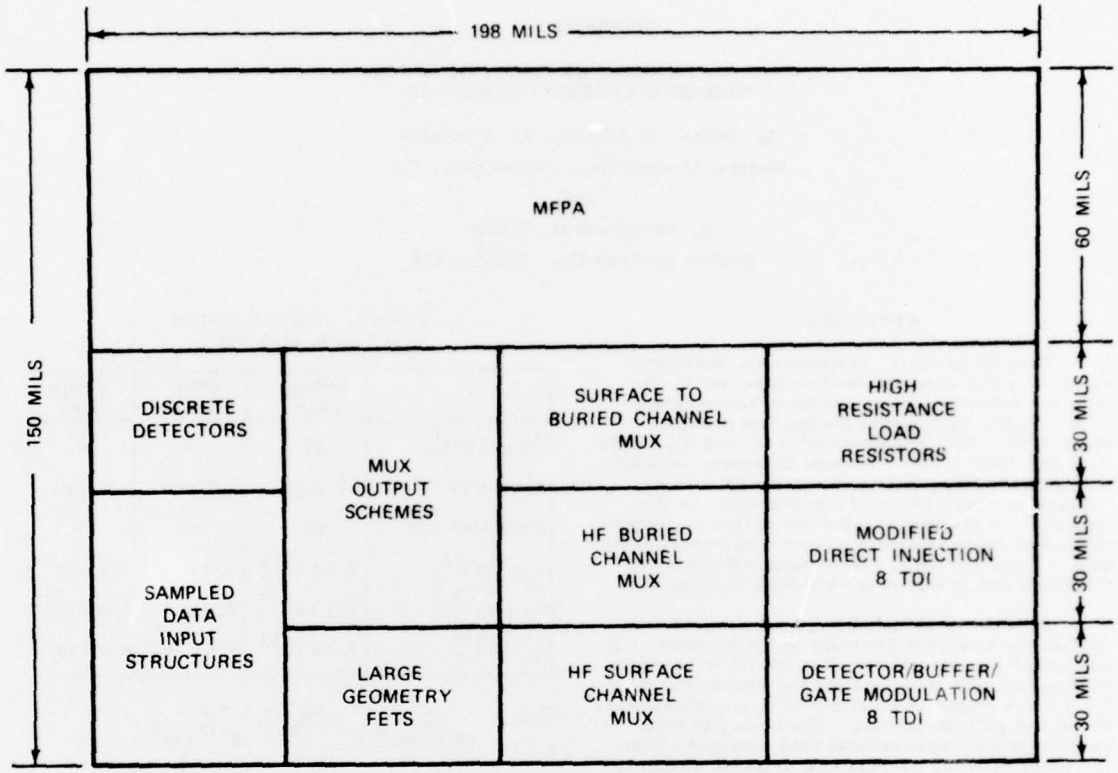

Figure 25. LADIR chip layout

APPENDIX

CHARACTERISTICS OF GALLIUM DOPED SILICON INFRARED DETECTORS

M. Pines, D. Murphy, D. Alexander
Hughes Aircraft Co., Culver City, CA
and
R. Baron and M. Young
Hughes Aircraft Co., Malibu, CA

ABSTRACT

Data on lifetime, responsivity, noise and detectivity has been obtained on discrete Si:Ga infrared detectors as a function of temperature (5 K - 35 K), background photon flux density ($\Phi_B = 10^{13} - 10^{17}$ photons/cm^2-sec) and bias field (E = 200-1200 v/cm). Several detectors with differing boron impurities and compensation were evaluated. The effects of compensation on the amplitude of the photoconductive lifetime, responsivity and noise is demonstrated with experimental data. From the data, the quantum efficiency of the detectors is shown to vary from 0.25 to 0.4.

A theoretical model has been developed to explain the observed behavior of the lifetime, signal, noise and detectivity. The model is based on solving the rate equations for the excess carriers for a three impurity level model (i.e., phosphorus, boron and gallium levels). The theory is compared with the experimental data obtained on the detectors showing correlation. Impulse response data on the Si:Ga detectors was obtained using a PbSnTe laser.

DATA ANALYSES

Material Characteristics

Hall samples were fabricated from the same wafers as the Si:Ga photoconductive detectors, yielding carrier concentration and Hall mobility of the detectors. The concentration of gallium, boron and phosphorus obtained from the data is shown in Table 1. These samples were chosen for further investigation because the gallium concentrations were very similar whereas the phosphorus concentration varied, allowing the establishment of the phosphorus dependence of responsivity, noise and detectivity. The detectors were fabricated from different portions of the same wafer. Previous tests have shown that variations of ±10 percent in the experimentally determined value of phosphorus are observed. Therefore the experimental data presented later will have this uncertainty associated with it.

To obtain the carrier concentration as a function of temperature and background photon flux the charge neutrality equation given by

Table 1. Characteristics of Si:Ga Detector

	3009A Tang	6001 Seed	3009A Seed
Length (mils)	20	20	20
Area (mils)	20 x 30	20 x 30	20 x 30
Thickness (mils)	40	40	40
N_{Ga} (cm^{-3})	2.3×10^{16}	3.3×10^{16}	2.7×10^{16}
N_B (cm^{-3})	1.1×10^{13}	2.9×10^{13}	1.4×10^{13}
N_p (cm^{-3})	7.1×10^{13}	1.5×10^{13}	4.6×10^{13}
$\sigma_{Ga_{th}} = 5.6 \times 10^{-16}$ cm^2		$\sigma_{B_{th}} = 1.8 \times 10^{-15}$ cm^2	
$\sigma_{Ga_{photo}} = 1.5 \times 10^{-6}$ cm^2		$\sigma_{B_{photo}} = 10^{-5}$ cm^2	

$$n_o + N_{Ga}^- + N_B^- = p_o + N_P^+ \quad (1)$$

must be solved where N_{Ga}^- is the concentration of ionized gallium atoms, N_P^+ is the concentration of ionized phosphorus atoms and N_B^- is the concentration of ionized boron atoms.

The concentration of ionized atoms for each of the three impurities is determined from the rate equation for each level which includes the thermal capture cross section and the photon capture cross section. The assumed cross sections for this analysis are given in Table 1. The result is a third order equation which upon solution yields the Fermi level, free carrier concentration, responsivity and lifetime.

Electrical Characteristics

The responsivity of an infrared detector is

$$R_I = \frac{I_s}{A_d H} \quad (2)$$

where H is the rms irradiance, I_s is the rms signal current, and A_d is the detector area. At low frequencies, it can be shown that the responsivity of an extrinsic photoconductive detector is[1]

$$R_I = \frac{q\eta_E\lambda}{hc}(N_A\sigma_A)\,G_o d = \frac{q\eta\lambda}{hc}G_o \qquad (3)$$

where

$$G_o = \frac{E\mu\tau}{\ell}, \quad \sigma_A = N_A\sigma_A \qquad (4)$$

$$\eta = \eta_I\eta_E, \quad \eta_I = N_A\sigma_A d \quad (\textit{for thin detectors}) \qquad (5)$$

Here λ is the peak wavelength, η is the quantum efficiency (i. e., I-internal, E-external), G_o is the d-c photoconductive gain, μ is the hole mobility, ℓ, w, and d are the length, width and thickness of the detector, σ_A is the photo capture cross section and N_A is the concentration of photon absorbing impurities.

For a photoconductive detector the generation-recombination noise spectrum at low frequency is[2,3]

$$I_{g\text{-}r} = 2Eq\mu\,(p\tau)^{1/2}\left(\frac{dw}{\ell}\right)^{1/2} \qquad (6)$$

where $p = p_o + p_e$, p_o is the concentration of thermal carriers, and p_e is the concentration of excess carriers.

When $p_e >> p_o$ (which it is during normal photoconductor operation) and since

$$p_e = g_E\tau = \eta\phi_B\tau/d,$$

where ϕ_B is the background photon flux density

$$I_{g\text{-}r} = 2q\left(\eta\phi_B A_d\right)^{1/2}G_o \qquad (7)$$

Detectivity is defined as

$$D^*_{\lambda_p} = \frac{R_I A_d^{1/2}}{I_n} \qquad (8)$$

where I_n is total noise (A/$\sqrt{\text{Hz}}$). The substitution of Equations (3) and (6) into Equation (8) gives

$$D^*_{\lambda_p} = \frac{\eta\lambda}{2hc}\sqrt{\frac{\tau}{pd}} \xrightarrow{p_e >> p_o} \frac{\lambda}{2hc}\sqrt{\frac{\eta}{\phi_B}} \qquad (9)$$

As can be seen from Equation (3), lifetime τ can be determined from responsivity data, i. e., the lifetime is

$$\tau = \frac{R_I hc\ell}{q\eta\lambda E\mu} \qquad (10)$$

where the value of η can be determined from D* data, μ from Hall measurements[4] and E, ℓ, h, λ and q are either knowns or variables of the experiment. R_I is obtained from measurements.

Figure 1 shows the calculated effect of lifetime, responsivity and noise on the concentration of phosphorus and gallium at a temperature of 20K. The responsivity varies more than the lifetime due to the quantum efficiency dependence on gallium concentration[5]. The case chosen is a background photon flux density of 1.5×10^{15} photons/cm^2-sec. The lifetime and responsivity are independent of background photon flux at this temperature. The theoretical results indicate that the lifetime, responsivity, and noise levels are dependent on the phosphorus concentration. This is because the lifetime is roughly given by

$$\tau = \sum_i \frac{1}{\alpha_i N_i}, \quad \alpha = \sigma_{th_i} V_{th} \qquad (11)$$

where σ_{th} is the thermal capture cross-section, V_{th} is the thermal velocity and i indicates the gallium or boron level.

The above analysis established the dependence of responsivity, lifetime, and noise. In the following section data will be presented and correlated with the theory.

Experimental Results

Figure 2 shows responsivity versus temperature and background photon flux density for three different detectors with different concentrations of phosphorus. Table 1 shows the various concentrations of gallium, boron and phosphorus. The Hall data indicates that the 6001 seed is undercompensated with $N_{\bar{p}} = 1.5 \times 10^{13}$ cm^{-3} and the 3001A Seed and Tang have a $N_{\bar{p}}$ of 4.6×10^{13} and 7.1×10^{13} cm^{-3} respectively. Figure 1 showed that theoretically the responsivity is expected to increase as the phosphorus concentration is decreased, which is consistent with the responsivity data shown in Figure 2. The theory also predicts that the responsivity is independent of background photon flux density at the lower temperatures. This is also shown by the data of the three detectors for the different background photon flux densities. As the temperature was increased towards 30K the responsivity tended to increase but never as much as the theory would indicate for the lower background photon flux densities. The peaking in responsivity at approximately 25K is caused by the Fermi level passing through the boron level causing thermalization of the boron level. The measurements at 25K and above became extremely difficult to obtain due to the rapidly varying impedance of the Si:Ga detectors. Some of the peaking expected at the lower backgrounds could have been masked by this difficulty. At the lower temperature and background the experimental data on responsivity is seen to increase but the theory doesn't predict this. This increase has previously been reported as a dip in the responsivity at the mid temperature range (and

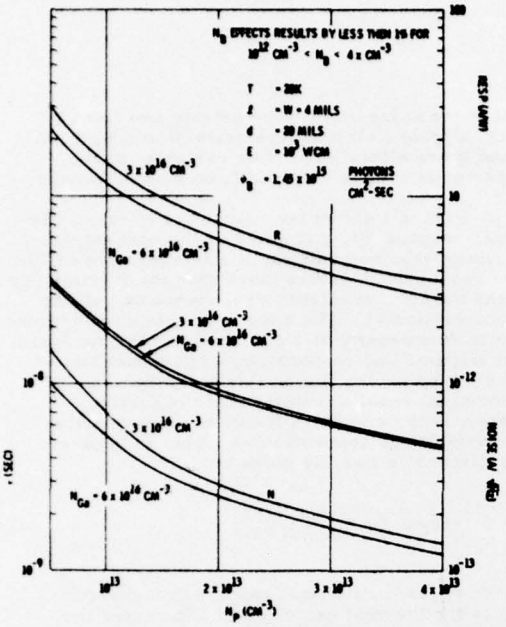

Figure 1. Responsivity, lifetime and noise as a function of phosphorous compensation

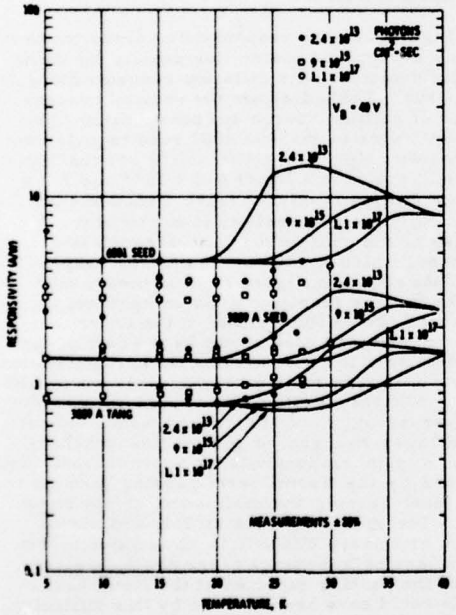

Figure 2. Responsivity versus temperature for various background photon flux densities

an increase at the lower and higher temperature). It seems that the increase in responsivity at the higher temperature can be explained but at lower temperatures the effect is not understood.

Figure 3 shows the detector noise versus temperature for various background photon flux densities. The data is in excess of the calculated noise. The discrepancy could be due to contact noise or to an extra g-r term that involves the boron level. Here again the noise is greatest when the phosphorous concentration is minimum and this is the case with 6001 Seed. The increase at higher temperatures is due to the increase of the majority carriers due to thermalization.

Figure 4 shows D* versus temperature for various background photon flux densities. As the theory shows, the more overcompensated the detector the high temperature at which BLIP (background limited infrared photodetection) performance is lost. This seems to indicate that for highest temperature operation overcompensated detectors are desirable. This result though must be traded off against the lower responsivity and noise level from the detectors. Figure 5 shows lifetime versus temperature. The experimental data was obtained from Equation 10 and Figure 2.

Figure 6 shows frequency response data as obtained with a pulsed PbSnTe laser emitting at 10.8 μm on detector 3009A Tang. The other two detectors ceased working due to failure at the contacts. No roll off was observed at the higher backgrounds up to frequencies of 1 MHz whereas at the lower background a 3-dB of 40 KHz was observed. This roll off is not consistent with the detector photoconductive lifetime or the dielectric

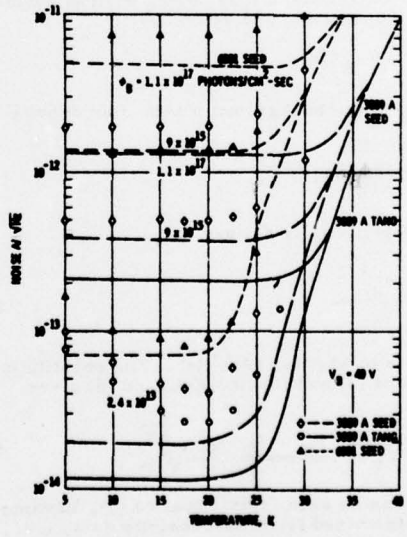

Figure 3. Noise versus temperature for various background photon flux densities

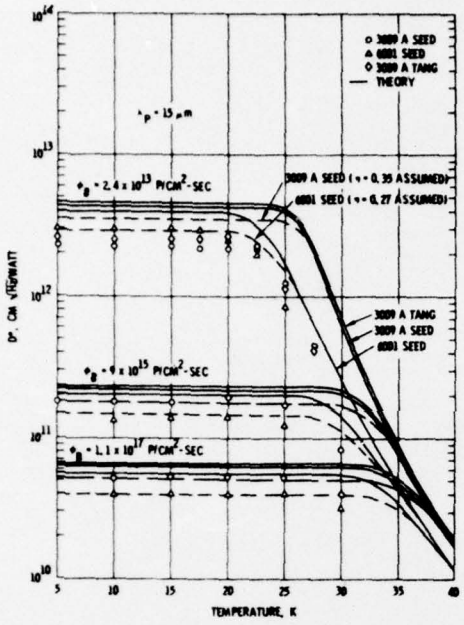

Figure 4. D* versus temperature for various background photon flux densities

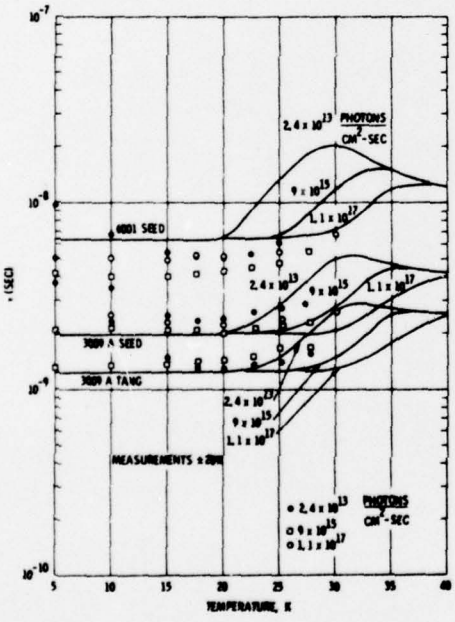

Figure 5. Si:Ga - Lifetime as a function of temperature for various background photon flux densities

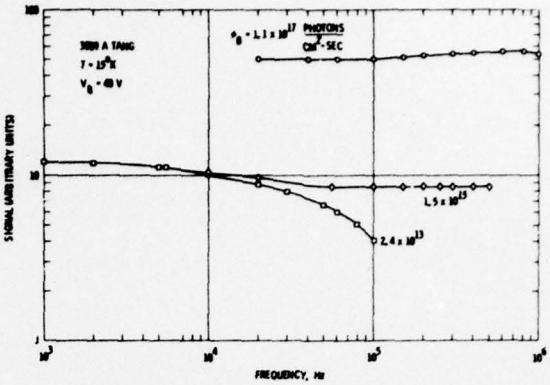

Figure 6. Si:Ga Signal response versus frequency for various background photon flux densities - PbSnTe - laser source

relaxation time (i.e., the photoconductor lifetime being sufficiently shorter and the dielectric relaxation time being significantly longer). The photoconductive gain at this bias is only approximately 0.2 and therefore no photoconductive gain saturation should be seen[6].

CONCLUSIONS

Data has been presented on Si:Ga photoconductors correlating the responsivity, noise, D* and lifetime dependence on the concentration of phosphorous, gallium and boron and a model has been presented explaining the observed behavior.

References

(1) Long, D., Infrared Physics, 7, 121 (1967).

(2) Long, D., Infrared Physics, 7, 169 (1967).

(3) Burgess, R., Proc. Phys. Soc., B68, (1955).

(4) Boron, R., private communication.

(5) Lucovsky, G., Solid State Commun., 3, 299 (1965).

(6) Milton, A. F. and Blouke, M. M., Phys. Rev. B, 3, 4312, (1971).

☆ U. S. GOVERNMENT PRINTING OFFICE: 1976 — 657-630/1038